

Abundance profiles and cool cores in galaxy groups

Ria Johnson^{1*}, Alexis Finoguenov², Trevor J. Ponman¹, Jesper Rasmussen³,
Alastair J. R. Sanderson¹

¹*School of Physics and Astronomy, University of Birmingham, Edgbaston, Birmingham B15 2TT, UK*

²*Max-Planck-Institut für extraterrestrische Physik, Giessenbachstraße, 85748 Garching, Germany*

³*Dark Cosmology Centre, Niels Bohr Institute, University of Copenhagen, DK-2100 Copenhagen, Denmark*

1 May 2018

ABSTRACT

Using data from the Two Dimensional *XMM-Newton* Group Survey (2dXGS), we have examined the abundance profile properties of both cool core (CC) and non cool core (NCC) galaxy groups. The ten NCC systems in our sample represent a population which to date has been poorly studied in the group regime. Fitting the abundance profiles as a linear function of log radius, we find steep abundance gradients in cool core (CC) systems, with a slope of -0.54 ± 0.07 . In contrast, non cool core (NCC) groups have profiles consistent with uniform metallicity. Many CC groups show a central abundance dip or plateau, and we find evidence for anticorrelation between the core abundance gradient and the 1.4 GHz radio power of the brightest group galaxy (BGG) in CC systems. This may indicate the effect of AGN-driven mixing within the central $\sim 0.1 r_{500}$. It is not possible to discern whether such behaviour is present in the NCC groups, due to the small and diverse sample with the requisite radio data. The lack of strong abundance gradients in NCC groups, coupled with their lack of cool core, and evidence for enhanced substructure, leads us to favour merging as the mechanism for disrupting cool cores, although we cannot rule out disruption by a major AGN outburst. Given the implied timescales, the disruptive event must have occurred within the past few Gyrs in most NCC groups.

Key words: galaxies: clusters: general - intergalactic medium - X-rays: galaxies: clusters

1 INTRODUCTION

The dominant baryonic mass component in galaxy groups and clusters is the hot X-ray emitting intracluster medium (ICM), with stellar mass becoming increasingly important as mass decreases (Gonzalez, Zaritsky & Zabludoff 2007; Giodini et al. 2009). Studying the metallicity of the ICM can provide insight into the processes that have shaped its thermodynamic history. The heavy elements observed in the ICM originate predominantly from supernovae explosions, which eject material into the ICM (Arnaud et al. 1992). Gas can also be removed from galaxies, thus enriching the ICM with metals, through processes such as ram-pressure stripping (Gunn & Gott 1972) and galaxy-galaxy interactions (see Schindler & Diaferio 2008, for a review of enrichment processes). The efficiency of any one transport process depends on the properties of both the galaxies and their large-scale environment (Schindler & Diaferio 2008, and references therein).

Using *ASCA* and *ROSAT* observations, Finoguenov & Ponman (1999) found the groups HCG 62 and NGC 5044 to have significant negative abundance gradients, a result also seen in the *ROSAT* sample of Buote (2000). The

abundance gradient in NGC 5044 was also observed by Buote et al. (2003) using *XMM-Newton* and *Chandra* data, and recent studies have shown the presence of an abundance gradient to be a common feature (e.g. Morita et al. 2006; Rasmussen & Ponman 2007; Tokoi et al. 2008; Komiyama et al. 2009; Sato et al. 2009). Rasmussen & Ponman (2009) also find a central excess of iron in all but two of their groups, the presence of which can be explained solely by supernovae Type-Ia products from the central galaxy. The excess extends beyond the optical limits of the central galaxy, as also seen in clusters (David & Nulsen 2008; Rasera et al. 2008). The re-distribution of enriched gas can be achieved by outflows from active galactic nuclei (AGN) (e.g. Mathews, Brighenti, & Buote 2004; Rebusco et al. 2006; Moll et al. 2007), the presence of which is commonly invoked to explain the lack of catastrophic cooling in the centres of groups and clusters.

The division of galaxy clusters into samples of cool core (CC) and non cool core (NCC) systems is well-established (e.g. Peres et al. 1998). Recent work has shown both CC and NCC galaxy clusters to show similar, steep abundance gradients (Sanderson, O’Sullivan, & Ponman 2009; Sivanandam et al. 2009). However, earlier observational work by De Grandi & Molendi (2001) indicated that NCC clusters have flat abundance profiles,

* Contact via: tjp@star.sr.bham.ac.uk

in comparison to the steep abundance gradients seen in CC clusters. The prevalence of merging systems in the NCC sample of this work led the authors to interpret mergers as a mechanism for re-distributing metals.

The division into CC and NCC classes has only recently been applied to study the properties of a sizeable sample of systems in the group regime (Johnson, Ponman, & Finoguenov 2009). The origin of NCC clusters remains an open question, given their short central cooling times (Sanderson, Ponman & O’Sullivan 2006), indicating that either the formation of cool cores in these systems has been suppressed, for example through pre-heating (e.g. McCarthy et al. 2008) or thermal conduction (e.g. Voigt & Fabian 2004), or the cores in NCC systems have been disrupted by mergers (e.g. Allen et al. 2001) or AGN heating (see the review by McNamara & Nulsen 2007). These physical processes scale differently with system mass, so we can gain significant insight into the origin of NCC systems by studying NCC groups. The abundance behaviour in NCC groups has not previously been studied in a sample of any size, and could prove a useful diagnostic in establishing the dominant physical processes influencing the ICM.

The layout of the paper is as follows. In Section 2 we describe the group sample and data analysis, in Section 3 we present the mean temperature profile of the CC and NCC groups and in Section 4 we present the abundance profiles of the CC and NCC groups. We discuss our results in Section 5 and present our conclusions in Section 6. Solar abundances are quoted as those of Anders & Grevesse (1989).

2 GROUP SAMPLE AND SPECTRAL ANALYSIS

Our sample of 28 galaxy groups is a combination of the groups with the highest quality *XMM-Newton* data from the Two-Dimensional *XMM-Newton* Group Survey (2dXGS) sample of Finoguenov et al. (2006, 2007) and the group sample of Mahdavi et al. (2005). Here we present a summary of the sample and the data analysis procedures, although we refer the reader to Johnson et al. (2009) for a detailed discussion of the group sample. Twenty-seven of the groups are situated within $z < 0.024$, with the final group at a redshift of 0.037 (RGH 80, see Mahdavi et al. 2005). The data reduction is described in detail by Mahdavi et al. (2005) and Finoguenov et al. (2006, 2007), but we present a brief summary of the approach here. Instead of a traditional annular spectral analysis, spectra were extracted from regions of contiguous surface brightness and temperature. This deprojection method involves no *a priori* assumption of spherical symmetry, but on the other hand it does not correct for emission from overlying layers of material. We refer readers to Mahdavi et al. (2005), Finoguenov et al. (2006) and Finoguenov et al. (2007) for full details.

Results from two spectral analyses are presented here. In the first, spectra were extracted in the range 0.5–3 keV and fitted with single-temperature (1T) hot plasma (APEC) models to yield the temperature T and abundance Z in each region. Deprojected values of entropy S and pressure P were calculated by assuming a length along the line-of-sight for each spectral region derived from its distance to the centre of the system. These results have already been used to examine the feedback properties of groups (Johnson et al. 2009).

Assuming a single temperature model in regions where a spread of temperatures is present, as may be the case within cool cores or where regions of different temperature are projected on top of one another, can lead to systematic underestimation of the

metallicity (Buote & Fabian 1998). To check for this, a second spectral analysis is performed, in which spectra are fitted with a two-temperature (2T) model, in which abundance is taken to be the same in both phases. To better constrain these 2T models, spectra were extracted across a wider energy range (0.5–7 keV). The original motivation for using a smaller energy range for 1T fits was to constrain the temperature primarily using the position of the lines, aiming to reduce bias in the metallicity arising from any distortion in the continuum. We concentrate here on the properties of the abundance profiles of groups, having already explored the diversity in group properties such as entropy, and the implications for feedback processes, in Johnson et al. (2009).

We are entering an era where large galaxy samples can be used to study the gas properties of galaxy groups (e.g. Rasmussen & Ponman 2007; Sun et al. 2009). In particular, Rasmussen & Ponman (2007, hereafter referred to as RP07) derived detailed temperature and abundance profiles for 15 systems, 14 of which were shown to host a CC. The size and diversity of our sample allows its division into CC and NCC systems (e.g. Peres et al. 1998), based on the properties of their observed temperature profiles. The groups in our sample were classified as CCs if the ratio of the temperature in the radial range $0.1\text{--}0.3 r_{500}$ to the temperature in the radial range $0.0\text{--}0.05 r_{500}$ was found to be greater than 1. This was found to be a successful discriminator between the systems showing central temperature drops and those which do not. Although not a statistically selected sample, the 18 CC and 10 NCC groups allow us to identify trends in properties based on this segregation – a first in the study of galaxy groups.

To negate the effects of the differing sizes of the systems under consideration, we have scaled radial measurements by r_{500} (measured in kpc), the radius within which the mean density is equal to 500 times the critical value. This was defined for the 2dXGS groups by Finoguenov et al. (2006, 2007) in the following way,

$$r_{500} = 0.391 \bar{T}^{0.63} h_{70}^{-1}, \quad (1)$$

where \bar{T} is the temperature (in keV) measured in the radial range $0.1\text{--}0.3 r_{500}$ using a single-temperature spectral model. The groups included in our work from the Mahdavi et al. (2005) sample have been re-analysed to extract \bar{T} and r_{500} .

2.1 Background Fitting Methodology

Our approach to the complex issue of removing the *XMM-Newton* background uses a fitting methodology that allows for the fact that the background is changing in time and space. The details of the background treatment adopted in obtaining the *XMM-Newton* results used in this work are presented by Finoguenov et al. (2007). We perform the standard subtraction of the quiescent background and allow for a soft component ($T \sim 0.2$ keV) to account for variations in the Galactic foreground. In order to fully describe the non-X-ray background, up to two power-laws were fitted in addition to the thermal model. These power-laws were not convolved with the effective area of the telescope, achieved using the ‘background’ model in XSPEC. In the X-ray faintest regions of groups this background component dominates at energies $E \gtrsim 3$ keV. In combination with the distinct continuum shape of the ~ 1 keV thermal group emission, this allows us to characterise this component in a robust and unbiased manner.

When computing uncertainties on fitted source parameters, all other parameters, including those associated with the fitted background model, were allowed to reoptimise. Hence, uncertainties on derived T and Z due to the background level are included in our

error budgets. This is a more flexible treatment of the background compared to that often employed for nearby galaxy clusters, where the background is inferred using different observations. In fitting cluster emission, a recent practice has been to add a systematic error due to the background subtraction. We have refrained from doing so, since we directly fit for local background shape in the spectral analysis. However, the faintest groups studied here (and those having short *XMM-Newton* exposures) cannot be traced to the edge of the *XMM-Newton* field-of-view, and therefore it is not possible to accurately fit the source spectrum and power-law component in these outer regions. Such zones are therefore excluded from our analysis.

To show the variation in data quality in the outermost regions used for abundance determinations, we plot in Figure 1 examples of the fitted spectra and background for two of the groups in our sample (NGC 507 and NGC 5171). These were considered to show typical ‘best’ and ‘worst’ cases, in terms of constraining both the line and continuum emission in the spectra. The Figure demonstrates that even in the worst case (NGC 5171), the line and continuum emission are well-constrained, and show that the source emission is clearly discernible from the background, indicating that we are not over-interpreting the data at large radius. To further test the robustness of our spectral results and guard against the possibility that the χ^2 -minimisation of our fits would become trapped in local rather than global minima, we also inspected the χ^2 contour maps in the T - Z plane for a number of groups and spectral regions. In all cases considered, only one minimum was seen, even for confidence ranges larger than 3σ .

3 TEMPERATURE PROFILES

To illustrate the key differences between the temperature profiles of CC and NCC groups, we have stacked and scaled radially to r_{500} the temperature profiles derived from the 1T spectral fits for each sub-sample to give typical profiles. We have removed the dependence on the size of the system by dividing the temperature profiles by the characteristic mean temperature (derived within the radial range 0.1 – $0.3 r_{500}$). We performed a local regression ‘loess’ fit to the CC temperature profiles, weighting these fits by the inverse variance of the temperature measurement at each point. The algorithm fits a two-degree polynomial function using weighted least squares in the local neighbourhood of each data point. The size of the neighbourhood is defined to include a specified proportion of the data, which then dictates the smoothness of the resulting fit. The distance to each neighbour is used to weight the fit at each point. For more information, we refer the reader to Cleveland (1979) and Cleveland, Grosse & Shyu (1992).

However, due to the diversity in the temperature profile properties of the NCC groups, the regression fit in this case was unsuccessful, and instead we divided the data into four radial bins, each containing between 24 and 25 data points. To make a direct comparison with the CC profile, we calculated a weighted mean of the scaled temperature points in each radial bin, and also calculated the standard error on the mean scaled temperature (i.e. the rms scatter of the n values falling in each bin, divided by \sqrt{n}), to show the typical behaviour of the NCC temperature profiles. These temperature profiles for the CC and NCC groups are shown in Figure 2. The standard error on the regression fit to the CC groups inflates at both small and large radius; this is simply due to the lower number of data points in these regions. The larger standard error at radii greater than $0.5 r_{500}$ reflects the increased variance arising from

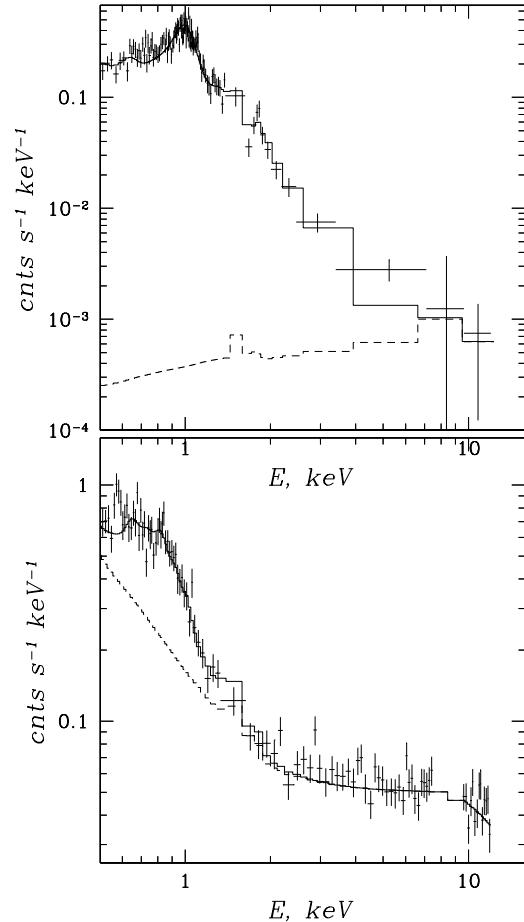


Figure 1. X-ray spectra (data points) and fitted source + background models (solid line) for the groups NGC 507 (top) and NGC 5171 (bottom). The dashed line shows the remaining background component once the standard background subtraction has been applied using blank sky fields. For both groups, these spectra were extracted from the outermost regions for which abundance determinations were possible.

larger measurement errors in this region of lower surface brightness. Figure 2 indicates a higher degree of consistency between the temperature profiles of CC systems, shown via the narrow standard error in comparison to the NCC systems.

4 ABUNDANCE PROFILES

Finoguenov & Ponman (1999) and Buote (2000) showed CC galaxy groups to have a central iron peak, a result confirmed for a larger sample of groups by RP07. However, the abundance profiles of NCC groups have not been previously investigated. Figures 3 and 4 show the abundance profiles from both 1T and 2T spectral fits, for both the CC and NCC groups in the 2dXGS sample. In both figures, the horizontal error bars show the radial width of each bin, and the vertical error bars show the measurement error derived from XSPEC, which takes into account the uncertainty on the modelled background.

As expected, the 2T models give higher metallicity, especially in regions from the which the spectrum is not well-represented by an isothermal plasma. This is especially the case within cool cores, where the steep gradient results in regions of differing temperature being projected on top of one another, and also thermal instability

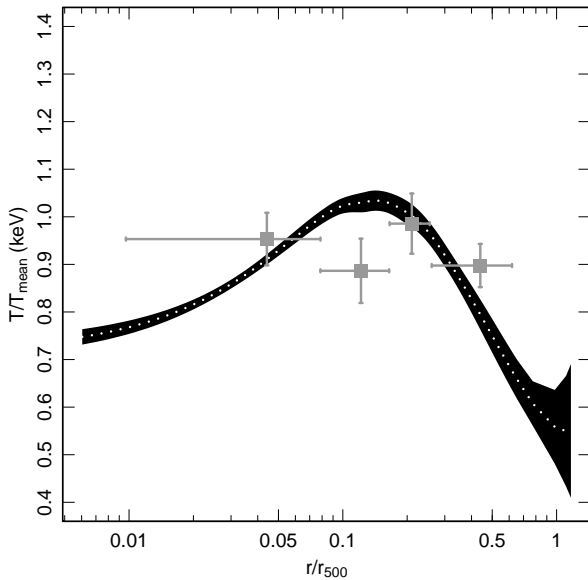


Figure 2. The typical temperature profiles from 1T spectral fits (scaled by the mean group temperature, measured in the radial range $0.1\text{--}0.3 r_{500}$) for CC groups (black confidence region and white dotted line) and for NCC groups (filled squares with error bars). The typical temperature profile in the CC case is derived via a weighted local regression fit, where the associated confidence region shows the standard error on the fit. The number of groups contributing to the CC profile falls to two at a radius of $0.6 r_{500}$, so the interpretation of the profile beyond this radius should be treated with caution. Due to poorer statistics in the NCC case, we have stacked the profiles into four radial bins, calculating the mean scaled temperature (grey squares) and the standard error on the mean scaled temperature (grey error bars).

may result in multiphase gas (Buote & Fabian 1998). We note that the results from 1T and 2T models converge at large radii, and the abundance offset between the two models is more significant in the case of CC groups, where the inferred abundance gradient is steepened by the use of a 2T model. NGC 5044 (see Figure 3) provides an especially striking example.

Abundance profiles in CC and NCC groups can be compared by stacking results from the groups in each subsample. We divided the radial range of the data for the CC and NCC systems into five equally spaced bins (in log space), and within each radial bin determined the mean abundance from the ensemble of results falling within this bin, and a standard error from their scatter. The result is shown in Figure 5. Results were derived separately for 1T and 2T fits, to illustrate the impact of the 2nd temperature component on the fitted abundances. The horizontal error bars in Figure 5 show the width of the radial bins used in the stacking analysis. The vertical error bars show the standard error for each radial bin. This is larger for 2T models, since the larger number of free parameters in the model leads to greater scatter in the results.

Figure 5 also shows the results of performing a linear regression on the original unbinned data for the CC and NCC samples separately. No statistical weighting has been applied when calculating these regression lines, since the variance about the mean profile is dominated by system-to-system variations, rather than statistical scatter. We fit linear models in log–linear space using the R function ‘LM’ for linear regression, finding the following relations, using 1T models, for the CC groups,

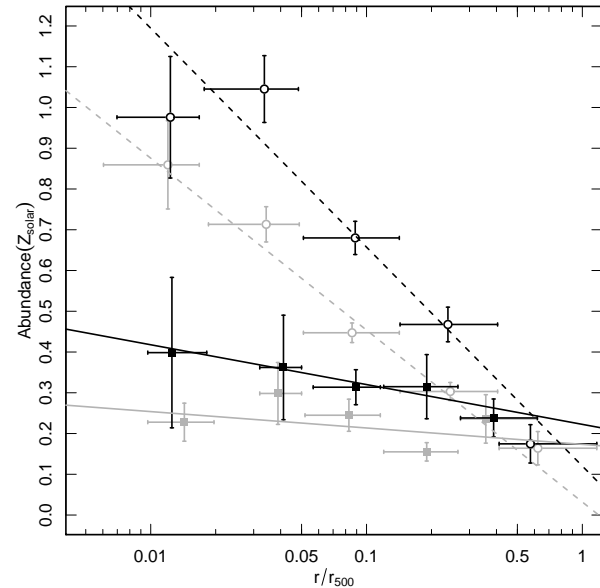


Figure 5. The stacked abundance profiles of the groups, divided into the CC (open circles) and NCC (filled squares) sub-samples. The results of the 1T fits are shown in grey, and the results of the 2T fits are shown in black. The vertical error bars are the standard error on the mean profile, and the horizontal error bars show the radial width of each bin. The dashed and solid lines are linear fits to the whole data set of abundances from the CC and NCC groups respectively, colour coded for the 1T (grey) and 2T (black) fits.

$$Z_{CC} = -0.42 (\pm 0.04) \log \left(\frac{r}{r_{500}} \right) + 0.03 (\pm 0.04) Z_{\odot}, \quad (2)$$

and for the NCC groups,

$$Z_{NCC} = -0.04 (\pm 0.05) \log \left(\frac{r}{r_{500}} \right) + 0.17 (\pm 0.05) Z_{\odot}. \quad (3)$$

Under the 2T spectral models, the fitted trend for the CC groups is,

$$Z_{CC} = -0.54 (\pm 0.07) \log \left(\frac{r}{r_{500}} \right) + 0.12 (\pm 0.07) Z_{\odot}, \quad (4)$$

and for the NCC groups,

$$Z_{NCC} = -0.10 (\pm 0.10) \log \left(\frac{r}{r_{500}} \right) + 0.22 (\pm 0.09) Z_{\odot}. \quad (5)$$

Clearly, the CC systems exhibit a much steeper abundance gradient, compared to the NCC systems. The fit to the NCC profiles is consistent with being flat within the quoted standard errors. This is true for both the fits from the 1T models and the 2T models. In the case of the CC profiles, results from 2T fits give a steeper slope than 1T models.

The group HCG 51 has a relatively high abundance in the 1T fits ($\sim 0.5\text{--}0.8 Z_{\odot}$) at radii between $0.3 r_{500}$ and $0.5 r_{500}$, which affects the calculation of the mean abundance in the outermost bin of the NCC profile in this case. To assess the impact of HCG 51 on this mean profile, we re-calculated the mean abundance in the outer bin, excluding HCG 51. This reduced the mean value to $0.14 \pm 0.02 Z_{\odot}$ from $0.24 \pm 0.06 Z_{\odot}$. Other bins are only marginally affected by the exclusion of HCG 51. Fitting a straight line model in log–linear space to the NCC groups, excluding all HCG 51 data, we find

$$Z_{NCC} = -0.09 (\pm 0.04) \log \left(\frac{r}{r_{500}} \right) + 0.10 (\pm 0.04) Z_{\odot}, \quad (6)$$

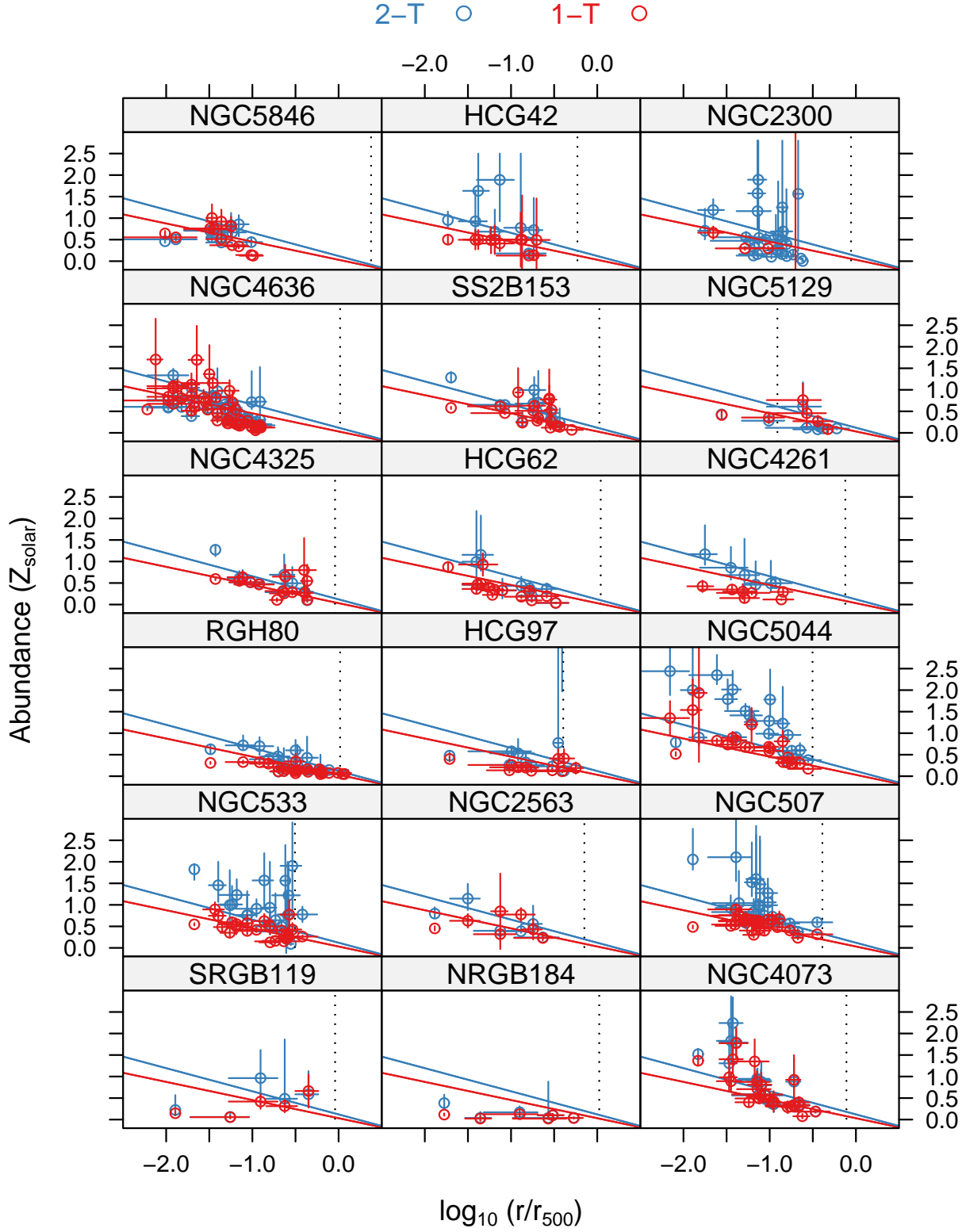


Figure 3. The abundance profiles of the CC groups in the 2dXGS group sample, shown in log–log space. The colours denote 1T (red) and 2T (blue) spectral fits. Vertical error bars are measurement errors and horizontal error bars show the width of each radial bin. The vertical dotted lines show the *XMM-Newton* field-of-view of $16'$ for all groups except NGC 4636 and NGC 5044, where the offset of the pointings shifts the outer boundaries to $18'$ and $17.7'$ respectively. The solid lines show the results of linear model fits to all CC groups, for both the 1T (red) and 2T (blue) spectral fits.

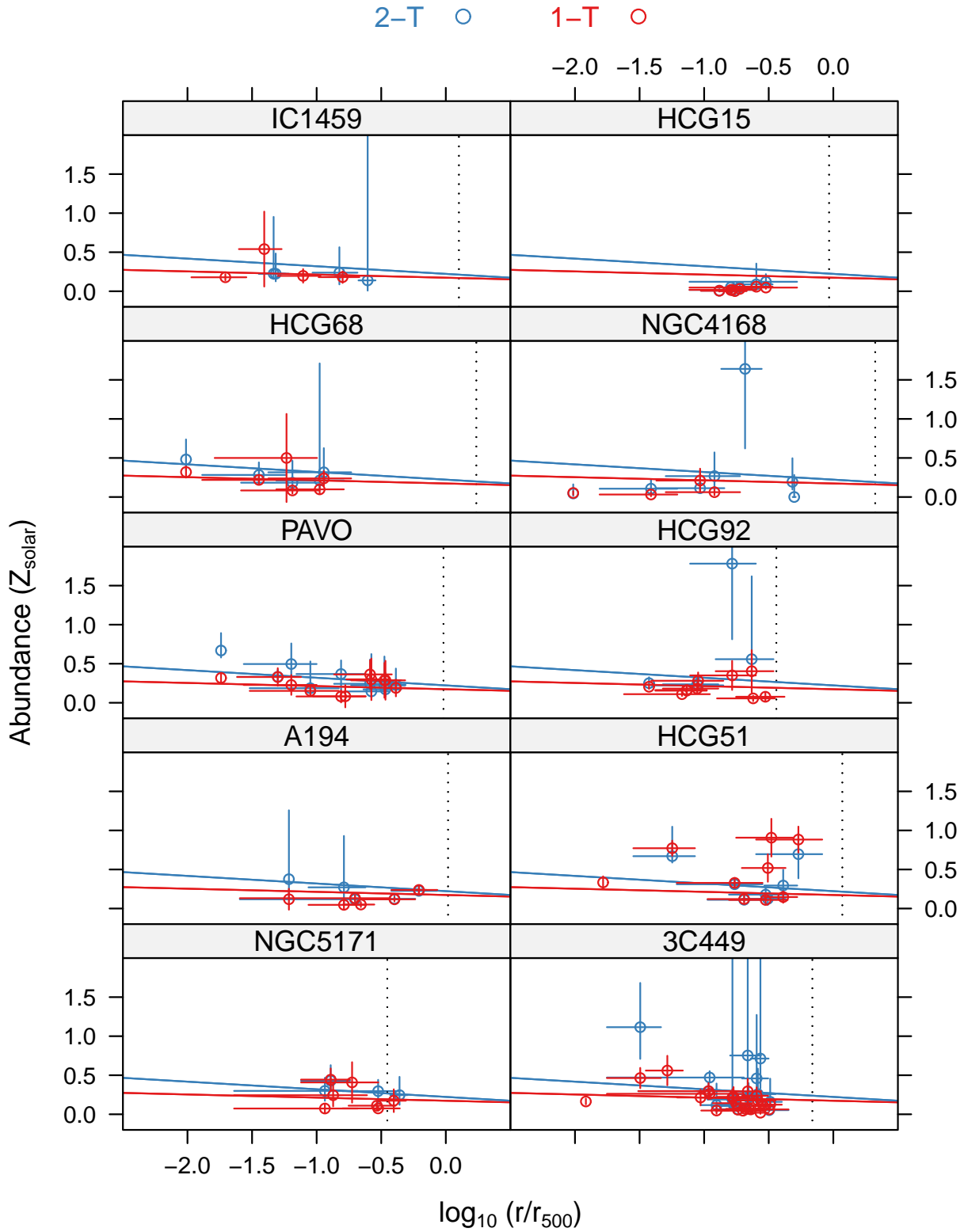


Figure 4. The abundance profiles of the NCC groups in the 2dXGS group sample, shown in log–log space. The colours denote 1T (red) and 2T (blue) spectral fits. Vertical error bars are measurement errors and horizontal error bars show the width of each radial bin. The vertical dotted lines show the *XMM-Newton* field-of-view of $16'$ for all groups. The solid lines show the results of linear model fits to all NCC groups, for both the 1T (red) and 2T (blue) spectral fits.

yielding a slope that is non-zero (within a 95% confidence interval), but still much shallower than that found in the CC systems. In the case of 2T spectral fits, excluding HCG 51 gives a mean profile for NCC groups

$$Z_{\text{NCC}} = -0.10 (\pm 0.11) \log \left(\frac{r}{r_{500}} \right) + 0.21 (\pm 0.10) Z_{\odot}, \quad (7)$$

with a slope which is consistent with zero within the 1σ error.

The presence of a central abundance peak is consistent with being built from the products of type Ia supernovae occurring in the central galaxy, in both groups (Rasmussen & Ponman 2009) and clusters (David & Nulsen 2008). However, the typical optical extent of the central group galaxy is only $0.05 r_{500}$, indicating that the metallicity profile of the CC and NCC systems continues to fall well outside the central galaxy. This suggests that metals have been expelled from the central galaxy into the surrounding intracluster medium. We estimate a mean gas mass weighted metal fraction for the CC and NCC groups by summing the product of the metallicity and gas mass over a series of radial shells, and dividing by the total gas mass contained within these shells. The gas mass was derived from β -model fits to the gas density profiles (see Johnson et al. 2009, for more information). The calculation of the metal fraction was limited to within $0.3 r_{500}$ to ensure consistent radial coverage between the groups, and this is also the radius where the CC and NCC profiles begin to converge within the uncertainties in Figure 5.

Applying this analysis to the results from the 1T models, we find a mean metal fraction for the CC groups of 0.29 ± 0.03 , where the error quoted is the standard error on the mean metal fraction, whilst for the NCC groups the mean metal fraction is 0.16 ± 0.02 , almost a factor of two lower. In the case of the 2T models, abundances are higher, but the mean metallicity in CC systems within $0.3 r_{500}$ is still double that for NCC groups. A key question is whether the central metals seen in CC groups are missing in NCC groups, or whether they have just been mixed out to larger radii. For most of the CC groups, we do not have good metallicity estimates outside $0.5 r_{500}$. We therefore adopt an abundance of 0.18 solar outside $0.3 r_{500}$, corresponding to the average behaviour. We then find the mean total metal mass inside $0.3 r_{500}$ to be typically one half of that in the radial range $0.3 r_{500} - r_{500}$. This is not an insignificant fraction, so mixing out the central metal peak should have a substantial impact on the outer regions. Thus, if the central metal peak has been mixed out to a large radius in NCCs, it would be expected to lead to a significant rise in metallicity in the outer regions, compared with what is seen in CC groups. Within the limits of our data, there is no evidence for this, except in the case of HCG 51. However, better quality spectral data extending to large radii is required to firmly establish whether or not a mixing scenario is viable.

4.1 CC/NCC definition

The CC/NCC definition employed by Johnson et al. (2009) compared the temperature profile behaviour in the radial range $0 - 0.05 r_{500}$ with that in the radial range $0.1 - 0.3 r_{500}$. Therefore, when we classify a group as a CC, we are referring to a classic cool core system, equivalent to the LCC systems of Sun et al. (2009), with a core typically extending to $\sim 0.1 r_{500}$. With this definition, any groups showing a central temperature drop on very small radial scales (< 10 kpc), would be classified as NCC. Such behaviour is seen in ≈ 20 per cent of systems in the *Chandra* sample of Sun et al. (2009), termed ‘coronae’ class systems by Sun et al. They possess a small cool region lying within the central galaxy. None

Table 1. The fitted intercepts, slopes and errors for models fitted to the 1T and 2T results with 3C449 and HCG 51 reclassified as CC systems.

		NCC	CC
1-T	Slope	-0.05 ± 0.05	-0.06 ± 0.12
	Intercept	0.13 ± 0.05	0.03 ± 0.03
2-T	Slope	-0.06 ± 0.12	-0.56 ± 0.06
	Intercept	0.24 ± 0.12	0.09 ± 0.07

of the CC systems in the *Chandra* sample of RP07 shows temperature drops on such small radial scales. Most importantly for this work is the observation by Sun et al. (2009) of compact cool regions within 10 kpc in 3C 449 and HCG 51, classified in this work as NCC systems. We tested the susceptibility of our results to the applied CC/NCC definition in these two systems by changing their designation and determining the abundance gradients of the resulting stacked CC and NCC profiles. Again fitting a linear model in log-linear space to the results from both the 2T models and the 1T models, we find the slope and intercept of the abundance profiles to be consistent with the original profiles within the stated errors, for both the CCs and the NCCs. The fitted intercepts and slopes are shown in Table 1. Therefore, even if 3C 449 and HCG 51 have their CC status reclassified, the results from the stacking analysis are not significantly affected.

4.2 Comparison to Rasmussen & Ponman (2007)

Although the detailed abundance profile behaviour of NCC groups has not been previously examined, we can compare the behaviour of the CC abundance profiles here with those of RP07. The latter work benefits from the higher spatial resolution available with *Chandra* data, so we cannot draw inferences here on the presence of the central (within $0.01 r_{500}$) drop in abundance seen by RP07. We can however, compare the overall trend seen in the CC systems. There is an overlap of 10 CC systems between this work and the sample of RP07, which further allows a comparison of the spectral analysis methods for those systems in common. RP07 fitted their spectra with 2T models wherever these gave a significant improvement in fit, which was often the case within the cool core. We therefore show the comparison with both our 2T and 1T results.

To enable a fair comparison, we convert the Grevesse & Sauval (1998) abundances presented by RP07 to Anders & Grevesse (1989); this requires dividing the former by a factor of 1.48 (as described by RP07). A further correction is required to allow for the difference in the method of calculating r_{500} in the two samples, as the RP07 r_{500} values are typically ~ 1.14 times greater than the values used here. We have scaled the r_{500} values of the RP07 sample down by this factor to compare to our work. We have again stacked the abundance profiles for the CC groups, this time increasing the number of radial bins to allow a more thorough comparison with the profile of RP07. We also now calculate the median in each bin, to avoid any bias from an individual group influencing the overall profile. Although the mean trends are well-established (see Figure 5), individual groups do show some deviations from these mean profiles. To indicate the degree of scatter in each bin in Figure 6 we plot (as error bars) the median absolute deviation in each radial bin.

Figure 6 shows the stacked abundance profile for the CC groups from the current sample under the 2T analysis, shown as solid squares, and the stacked abundance profile from the sample of RP07, shown as open circles. The points from this analysis tend to be higher than those of RP07, however the spread of abundances

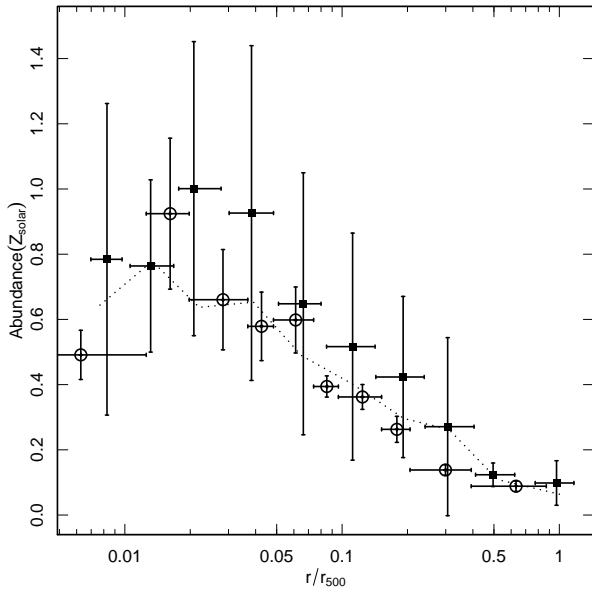


Figure 6. The stacked abundance profiles of the CC groups from our sample using the 2T analysis (solid squares), derived from the median abundance in each radial bin, with error bars that correspond to the median absolute deviation to show the degree of scatter in each bin. Open circles show the results of Rasmussen & Ponman (2007), where we have re-scaled their abundances by 1.48 to match the Anders & Grevesse (1989) abundances presented here, and have re-scaled the r_{500} values of Rasmussen & Ponman (2007) to allow for differences in the method of calculation. The dotted line shows the median abundances from the 1T spectral fits.

in each bin is much larger. It is worth noting that RP07 use VAPEC spectral models in XSPEC, so that the abundance shown in Figure 6 is actually the iron abundance. Within the RP07 sample, the difference between iron abundance and the mean metallicity is at most 15%. Since RP07 used a mixture of 1T and 2T spectral fits within their group cores, we also include our 1T profile in the Figure. In general, the shape of our mean abundance profile is consistent with that of RP07, though the match is closer for our 1T fits.

4.3 Comparison to clusters

Recent work on the abundance profiles of CC and NCC clusters has shown them to exhibit very similar profiles. For example, an analysis of *Chandra* data by Sanderson et al. (2009) showed NCC clusters to show a similar decline with radius to CC clusters, and Sivanandam et al. (2009) find steep abundance gradients in 9/12 clusters, of which only 4 are CCs. At intermediate redshift ($0.1 < z < 0.3$), Baldi et al. (2007) showed the abundance profiles of CC clusters to rise above those of NCC systems within $0.1 r_{180}$, however, outside this radius, they found no significant difference in the profiles of CC and NCC clusters. Earlier work by De Grandi & Molendi (2001) and De Grandi et al. (2004) with *BeppoSAX* data showed almost flat abundance profiles in NCC clusters, compared to steep abundance profiles in CC clusters. However, the NCC sample used in the *BeppoSAX* study consisted of well known merging clusters, which probably accounts for the different profiles in these compared to more recent studies of NCC clusters (S. Molendi, private communication).

In Figure 7 we compare the mean abundance profiles for the

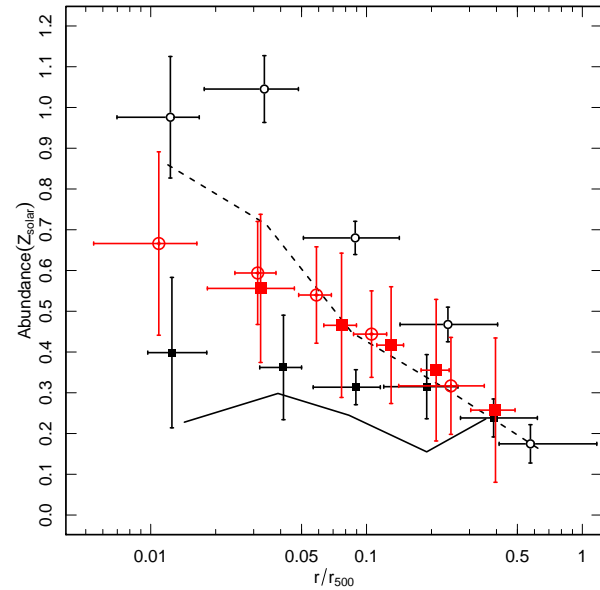


Figure 7. The stacked abundance profiles of the CC groups (open circles) and NCC groups (filled squares) from the 2T spectral fits, with vertical error bars showing the standard error on the mean abundance, and horizontal error bars showing the radial width of the bin. For comparison, we show the mean abundance profiles from the cluster sample of Sanderson et al. (2009) in red, with open circles denoting CC clusters and filled squares denoting NCC clusters. The horizontal error bars show the radial width of each bin, and vertical error bars show the standard deviation in each bin. We have re-scaled the abundances of Sanderson et al. (2009) to match the Anders & Grevesse (1989) abundances presented here. The dashed and solid lines show the mean results of our 1T spectral fits for CC and NCC groups respectively.

CC and NCC groups in our sample with the mean abundance profiles of a sample of 20 clusters, presented by Sanderson et al. (2009). The latter profiles have also been split into CC and NCC categories, and result from single-temperature fits to spectra extracted from annuli. Figure 7 shows the striking similarity between the abundance profiles of CC and NCC clusters, in contrast to the situation in groups, where CC and NCC systems have distinctly different profiles. Comparing CC groups to CC clusters shows CC groups to have a higher central peak, whether 1T or 2T models are employed, which may be explained by the increased dominance of the brightest group galaxy (BGG) in lower mass systems (e.g. Lin & Mohr 2004). NCC groups however have considerably flatter abundance profiles than NCC clusters. We will return to this point in Section 5.

4.4 Low abundance systems

Motivated by the challenge of determining the main driving factors that lead to the apparent bimodality in the abundance profiles presented in Section 4, we have looked for systems that buck these mean trends. We find four systems to have very low abundances of less than $0.2 Z_{\odot}$ across the measured radial range. Three of these groups are NCCs (HCG 15, NGC 4168 and A 194) and one is a CC system (NRGb 184). Given the role of the BGG in establishing the central peak in abundance (e.g. David & Nulsen 2008; Rasmussen & Ponman 2009), we hypothesise that these low abun-

dance systems have relatively small (i.e. lower stellar mass) brightest group galaxies, such that the relative injection of metals from the BGG is low.

We can assess this by calculating the ratio of the K -band luminosity of the BGG to the total gas mass within $0.3 r_{500}$. We estimate the K -band luminosity of the BGGs using K_{20} magnitudes from 2MASS (Skrutskie et al. 2006), assuming a K -band absolute magnitude for the Sun of 3.39 (Kochanek et al. 2001). The only system for which we do not have a K -band magnitude for the BGG is HCG 51. The gas mass comes from β -model fits to the gas density profiles of the individual groups (see Johnson et al. 2009, for more information). Simply measuring the mean $L_K(\text{BGG})/M_{\text{gas}}$ of these low abundance systems we find $L_K/M_{\text{gas}} = 0.38 \pm 0.07 L_{\odot,K} M_{\odot}^{-1}$, compared to the remainder of the sample for which $L_K/M_{\text{gas}} = 0.74 \pm 0.12 L_{\odot,K} M_{\odot}^{-1}$, where quoted errors are the standard error on the mean.

This indicates that the low abundance systems do indeed have a smaller ratio of stellar to gas mass within $0.3 r_{500}$. Is this sufficient to account for their lower metallicity? To assess this, we calculate the ratio of integrated iron to total stellar mass, to see whether it is abnormally low in the low abundance groups. Computing the product of gas mass and metallicity summed over a series of radial shells out to $0.3 r_{500}$, and dividing by the K -band luminosity of the BGG, gives an indication of the metal contribution from the BGG. In the low abundance systems, the mean of this ratio of ‘metal mass’ to $L_{K,\text{BGG}}$ is $0.19 \pm 0.03 Z_{\odot} M_{\odot}/L_{\odot,K}$, whilst for the remainder of the systems, it is $0.59 \pm 0.08 Z_{\odot} M_{\odot}/L_{\odot,K}$, where the errors quoted are the standard errors on the mean. This shows that the lower stellar mass of the BGGs in the low abundance groups is not sufficient to account for their low metal mass – the ratio of metal mass to stellar mass is actually lower in these systems. The same conclusion is arrived at if we allow for the possible contribution of non-central group galaxies to the metal mass within $0.3 r_{500}$. Using the total B -band luminosities within r_{500} from Johnson et al. (2009) to normalise metal mass we obtain a ratio for the low abundance systems of $0.21 \pm 0.06 Z_{\odot} M_{\odot}/L_{\odot,B}$, whereas the mean ratio is $0.91 \pm 0.12 Z_{\odot} M_{\odot}/L_{\odot,B}$ for the remainder of the sample. We conclude that the member galaxies in these low abundance groups contribute an unusually low metal mass to the ICM within $0.3 r_{500}$.

4.5 AGN activity

A statistical study of the effects of AGN activity on the gas properties of galaxy groups by Jetha et al. (2007) showed that although AGN may have an impact on the *local* gas properties, the large scale gas structure appears not to be significantly affected. The sample used by Jetha et al. (2007) was biased towards hotter systems with larger X-ray luminosities than ours. The majority of systems in the sample of Jetha et al. (2007) show a temperature decline within $0.1 r_{500}$ (see figure 4 in Jetha et al. 2007), indicating that their sample is dominated by CC groups. Here we have the advantage that we can consider the effects of AGN activity on NCC systems as well.

A study of the effects of feedback on the 2dXGS sample (Johnson et al. 2009) concluded that AGN are probably the dominant source of feedback, rather than supernovae, due to the lack of extra metals in systems with higher levels of feedback, but that much of this feedback might have taken place at earlier epochs. To investigate the effects of *current* AGN activity in these systems, we have extracted 1.4 GHz radio fluxes for the BGGs from the references shown in Table 2, primarily through the NASA/IPAC

Table 2. The mean group temperatures (measured in the region $0.1-0.3 r_{500}$) from 1T spectral fits, and the 1.4 GHz radio luminosity of the BGG. The final column shows whether the group was classified as CC or NCC by Johnson et al. (2009).

Group	T (keV)	$\log L_{1.4\text{GHz}}$ (W Hz $^{-1}$)	Radio ref.	CC/NCC
3C449	1.28±0.02	24.31	C02	NCC
A 194	1.01±0.15	23.85	C02	NCC
HCG 15	0.62±0.04	21.70	C02	NCC
HCG 42	0.75±0.19	21.09	C98	CC
HCG 51	1.16±0.13	–	–	NCC
HCG 62	1.06±0.02	21.51	C05	CC
HCG 68	0.69±0.09	21.91	C02	NCC
HCG 92	0.79±0.24	–	–	NCC
HCG 97	1.20±0.05	–	–	CC
IC 1459	0.59±0.03	23.02	C98	NCC
NGC 507	1.34±0.01	22.77	C02	CC
NGC 533	1.26±0.01	22.30	C02	CC
NGC 2300	0.75±0.01	20.47	C02	CC
NGC 2563	1.31±0.05	–	–	CC
NGC 4073	1.87±0.05	–	–	CC
NGC 4168	0.77±0.31	20.99	C02	NCC
NGC 4261	1.11±0.02	24.60	C02	CC
NGC 4325	1.01±0.01	–	–	CC
NGC 4636	0.77±0.01	20.97	C02	CC
NGC 5044	1.21±0.01	21.66	C05	CC
NGC 5129	0.95±0.03	22.01	C02	CC
NGC 5171	1.21±0.05	–	–	NCC
NGC 5846	0.69±0.01	21.36	C02	CC
NRGb 184	1.37±0.09	23.92	C02	CC
Pavo	0.77±0.12	–	–	NCC
RGH 80	1.16±0.02	23.40	C98	CC
SRGb 119	1.34±0.07	23.90	C02	CC
SS2b 153	0.83±0.01	21.66	C02	CC

References:

C98 – Condon et al. (1998)

C02 – Condon, Cotton, & Broderick (2002)

C05 – Croston, Hardcastle & Birkinshaw (2005)

Extragalactic Database (NED). Radio fluxes were not available in all cases, and we further searched the NRAO VLA Sky Survey (NVSS; Condon et al. 1998) around the BGG position for radio sources. The radio fluxes were converted to radio luminosities, and are shown in Table 2. The sample with available radio power estimates consists of 14 CC systems and 6 NCC systems.

The observed flatter abundance profiles in NCC galaxy groups compared to CC groups suggests that a mixing process may be affecting the gas distribution. If the source of this mixing were AGN, we might expect a correlation between a flatter abundance gradient and the presence of a powerful radio source. The 1.4 GHz radio power measures current AGN activity rather than recent activity, so the possibility of a time lag needs to be borne in mind. In Figure 8 we plot the observed abundance gradient within the group core from the 2T fits versus the 1.4 GHz radio luminosity for the systems where this latter measurement was available, separating the systems into CC and NCC groups. We specify the core abundance gradient as the ratio of the mean abundance measured within $0.05 r_{500}$ to that measured in the $0.1-0.2 r_{500}$ radial range. This choice is motivated by the observation of approximately flat abundance profiles inside $0.05 r_{500}$ in CC groups, observed by RP07. This also allows the abundance gradients to be measured across the same radial range in all systems. For the group NGC 5129, no data are available in the range $0.1-0.2 r_{500}$, so we take the mean

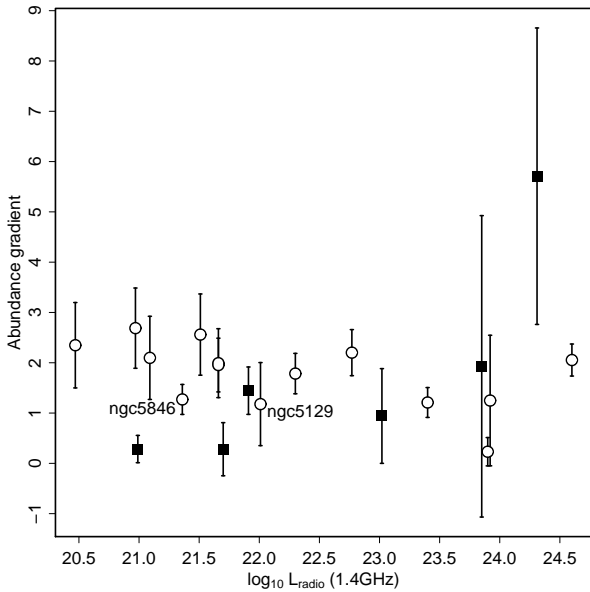


Figure 8. The measured abundance gradient within $0.2 r_{500}$ from the 2T spectral fits (see text) as a function of the logarithmic 1.4 GHz radio power of the brightest group galaxy. Open circles show CC systems, and filled squares show NCC systems. NGC 5129 and NGC 5846 are marked due to the difference in methodology for the calculation of the abundance gradient.

abundance in the range $0.2\text{--}0.3 r_{500}$ as the outermost measurement. Given the drop in abundance with radius in the CC systems, this should lead to an overestimate of the true abundance gradient by ~ 35 per cent. The group NGC 5846 also does not contain any data in the larger radial range, so we use the outermost abundance measurement instead, leading to a potential under-estimate of the abundance gradient. These data points are identified in Figure 8. Two of the NCC systems with measured radio luminosities have no abundance measurements within $0.05 r_{500}$. In these cases, we adopt a value within $0.05 r_{500}$ equal to the innermost measurement available. This assumes the innermost abundance profile is flat, which from Figure 5 is a reasonable assumption. In this scheme, a larger number on the y-axis in Figure 8 indicates a steeper abundance gradient.

The radio luminosities of the brightest group galaxies in the NCC groups cover a similar range to those in the CC groups. It is therefore immediately clear that current AGN activity is not responsible for the observed difference in abundance distribution between CC and NCC groups. For the CC groups, we find anticorrelation at the 95% confidence level between the core abundance gradient and radio power. A correlation test yields $\tau = -0.4$, with a p-value of 0.04. In the case of NCC groups, there is weak evidence for a positive correlation, but this is driven by the two groups with highest radio luminosity, which have very poorly determined abundance gradients. Better data are therefore required to draw any conclusions about any relationship between radio power and abundance distribution in NCC systems.

Considering just the CC groups, we can also look for any impact from the central radio sources on the temperature distribution. Johnson et al. (2009) calculated the temperature gradient from 1T spectral models, measured from the temperature peak to the temperature at $0.01 r_{500}$. This allows a calculation of the temperature gradient inside the temperature peak. Performing a Kendall correla-

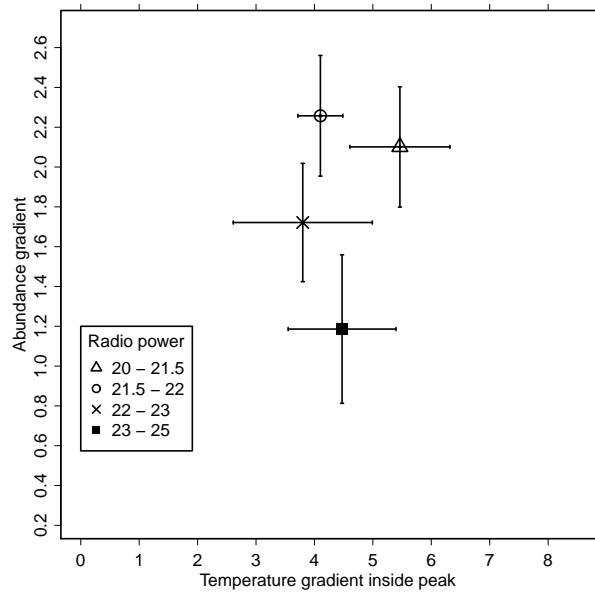


Figure 9. The abundance gradient (measured as explained in Section 4.5) versus the temperature gradient within the temperature peak from Johnson et al. (2009), for the CC systems. The 14 CC groups with available radio powers have been binned by the logarithm of their 1.4 GHz radio power, as described by the legend.

tion test between the logarithmic 1.4 GHz radio power of the BGG and the temperature drop inside the core (normalised by the mean temperature of the system), we find no significant correlation. In Figure 9 we show the abundance gradient (calculated as for Figure 8) versus the temperature gradient in the CC systems. Here we have split the groups into four bins in the logarithm of the 1.4 GHz radio power. Looking at these two parameters in conjunction with the abundance gradient measurement, steeper metallicity gradients occur in the cores of the systems with lower radio power, as was suggested by Figure 8. Figure 9 also confirms that the temperature gradient shows no strong trend with radio power.

To further investigate the relationship between AGN activity and abundance profiles, we sub-divide the 20 groups for which radio luminosities are available into ‘radio loud’ and ‘radio quiet’ sub-samples based on the median logarithmic radio luminosity of the whole sample ($\log L_{1.4\text{GHz}} = 21.96 \text{ W Hz}^{-1}$). The number of groups in each category is shown in Table 3. We show the stacked abundance profiles for the CC radio loud/radio quiet samples in Figure 10, derived from the 2T fits. The small number of groups in the radio loud and radio quiet NCC samples, and the diverse properties of these groups, preclude us from being able to draw any reliable conclusions on the effect of a central radio source in NCC systems, so we show the mean NCC abundance profile from Figure 5 in Figure 10. The profiles of CC groups with radio loud and radio quiet BGGs are quite similar. In particular, the central abundance levels (within $0.05 r_{500}$) are comparable, and both sub-samples seem to show a relatively flat profile within this radius. The large standard errors apparent in Figure 5 within the inner bins reflect considerable group-to-group diversity, as is apparent from examination of Figure 3. It can be seen that many CC groups show a plateau or decline in abundance at small radius, whilst others do not. This diversity makes the formal significance of the central flattening in abundance marginal within the stacked data. It is worth

Table 3. The breakdown of CC and NCC groups into the ‘radio quiet’ and ‘radio loud’ sub-samples.

	CC	NCC
Radio quiet	7	3
Radio loud	7	3
Total	14	6

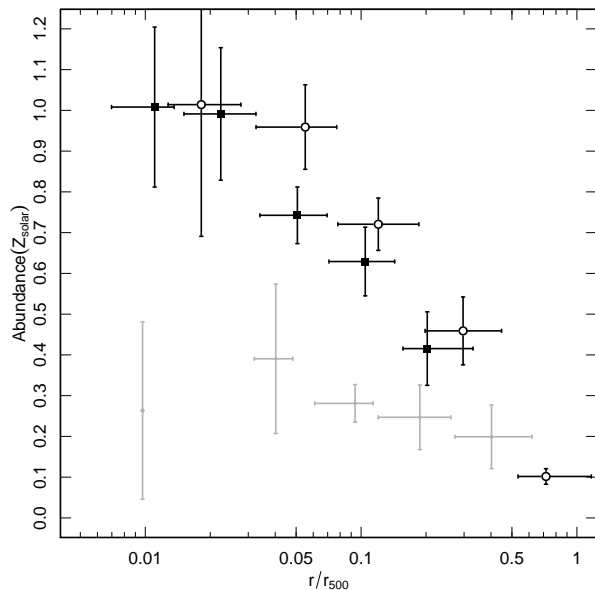


Figure 10. The stacked abundance profiles (from the 2T fits) of the CC sample (black), calculated from the mean in each radial bin, divided into those systems with ‘radio quiet’ BGGs (filled squares) and ‘radio loud’ BGGs (open circles). The mean profile of NCC systems from Figure 5 is shown as grey errorbars. Vertical error bars show the standard error of the mean profile and horizontal error bars show the radial width of each bin.

recalling that RP07, using higher spatial resolution *Chandra* data, found a central dip in abundance in most of their CC-dominated group sample. Dividing our sample by radio loudness, it can be seen from Figure 5 that there is some indication that the central abundance ‘plateau’ in radio loud BGGs may extend further (to $\sim 0.1 r_{500}$) than for radio quiet BGGs (to $\sim 0.05 r_{500}$).

4.6 Substructure

One way of destroying CCs is through mergers, which disrupt the ICM, mixing the gas. There is observational evidence to support this picture (e.g. Sanderson, Edge & Smith 2009). To test the hypothesis that NCC groups have had their CCs destroyed by mergers, we can look for substructure indicative of such events in our group sample.

Finoguenov et al. (2007) measured the level of substructure for 14 of the systems in our sample, by computing the entropy and pressure dispersion from the mean radial profiles. These gas properties were derived from 1T spectral fits, but in regions where the gas exhibits a range of temperatures, the 1T fit gives a temperature estimate which is essentially an emission-weighted mean, and the derived values of pressure and entropy are also reasonable estimates of the true values within the region. Figure 11 shows the entropy dispersion versus the pressure dispersion for the 14 groups

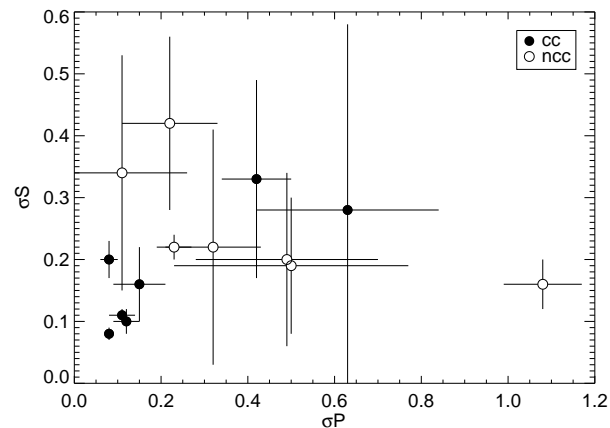


Figure 11. The dispersion in entropy versus pressure from the mean radial profiles calculated by Finoguenov et al. (2007) for 14 of the groups in our sample. Filled circles show CC systems, and open circles show NCC systems. The NCC systems show marginally more substructure (see text).

presented by Finoguenov et al. (2007). Examining the mean dispersion levels in the CC and NCC groups, we find a mean pressure dispersion of 0.23 ± 0.08 and 0.42 ± 0.12 respectively, a difference that is marginally significant (1.3σ). The mean dispersion in entropy for CC and NCC groups is 0.18 ± 0.04 and 0.25 ± 0.04 respectively, which has similar significance (1.4σ). The majority (5/7) of the CC groups cluster at low values of entropy and pressure dispersion. The two outlying CC systems are HCG 42 and NGC 4325. Finoguenov et al. (2007) identify NGC 4325 as deviating strongly from the mean pressure and entropy profiles, with a strongly peaked surface brightness profile. HCG 42 on the other hand is identified as a ‘normal’ group, albeit with a region of enhanced pressure and reduced entropy to the east of the group centre (Finoguenov et al. 2007).

We are dealing with less than half the group sample here, but there is tentative evidence to suggest a higher level of dispersion in both pressure and entropy in NCC systems. This indicates that the ICM in these systems shows more substructure. This might result from recent large scale disturbance of the gas in NCC groups, such as could be produced by a merger or possibly a major AGN outburst. However, we note that the NCC groups examined here are typically cooler than the CC groups, and so should have shallower group potential wells. Hence the ‘lumpiness’ due to the individual galaxy members will be greater in the NCC systems, and this may in turn contribute to the scatter seen in entropy and pressure. Applying a Kendall rank coefficient correlation test to test for a correlation between the group temperature and the entropy dispersion shows no significant correlation; however, performing the same test on group temperature and pressure dispersion, we find a highly significant anticorrelation – cooler groups tend to have higher pressure dispersion. The correlation test returns a value for τ of -0.57 and a p-value of < 1 per cent. The pressure may therefore be responding to the increased ‘lumpiness’ of the group potential in lower temperature systems.

A further avenue for exploring substructure is to consider the motion of the BGG relative to the rest of the group. Central dominant galaxies in clusters with evidence for substructure tend to have large peculiar velocities (Bird 1994). To probe the dynamical disturbance of CC and NCC groups, we calculated the absolute difference between the velocity of the BGG and the mean velocity of the remaining group members. In CC groups, we find a mean velocity

offset of $136 \pm 26 \text{ km s}^{-1}$, whereas for NCC groups we find a mean velocity offset of $218 \pm 80 \text{ km s}^{-1}$, where the errors quoted are the standard errors on the mean velocity offsets. Typically, brightest cluster galaxies have a peculiar velocity of approximately one third the velocity dispersion of their host cluster (Coziol et al. 2009). The typical velocity dispersion of our group sample is $\sim 400 \text{ km s}^{-1}$, making the velocity offset seen in CC groups consistent with this observation. However, NCC groups show a higher velocity offset, which may again indicate a higher level of dynamical disturbance in comparison to CC groups.

5 DISCUSSION

There is a clear difference in the stacked abundance profile properties of CC and NCC galaxy groups. Considering the linear fits to the raw data points (shown in Figure 5), we find the NCC systems to show approximately flat abundance profiles, compared to the steep gradients observed in the CC systems. Excluding the group HCG 51, which has abnormally high abundance at large radii in the 1T fits, increases the abundance gradient, but this remains much shallower than that observed in the CC systems, and remains consistent with a flat profile in the 2T fits. The abundance profiles of NCC groups also contrast sharply with those of NCC clusters, as shown in Figure 7.

All groups might be expected to possess cool cores, given their short central cooling times – typically a few Gyr at $0.05 r_{500}$ (O’Sullivan et al, in prep). One would also expect metallicity gradients in undisturbed groups: given the luminosities of their BGGs, type Ia supernovae products should be available to build the central metal peak on a timescale of $\sim 5 \text{ Gyr}$ (Rasmussen & Ponman 2009). The difference in the abundance profiles between CC and NCC groups, most notably the lack of a central peak in NCC groups, therefore suggests that gas in NCC groups has been vigorously mixed within the past few Gyr.

Rasmussen & Ponman (2009) found evidence that galaxies in low-mass ($T \lesssim 1 \text{ keV}$) groups are less efficient at releasing metals than those in more massive groups. This could help to explain the lower central abundances seen in NCC systems, since the NCC groups in our sample are typically cooler than the CCs, although there is a substantial overlap in the temperatures of the two sub-samples (Johnson et al. 2009). To remove any systematic effect associated with temperature, we removed the hottest and coolest groups from our sample, leaving sub-samples of 13 CC groups and 8 NCC groups spanning the same temperature range. These two trimmed sub-samples have very similar mean temperatures ($0.98 \pm 0.06 \text{ keV}$ for CCs, and $0.96 \pm 0.08 \text{ keV}$ for NCCs). The stacked abundance profiles of these trimmed sub-samples are shown in Figure 12, and are very similar to those for the full CC and NCC samples, shown in Figure 5, although the innermost point for this subset of CC groups has dropped by approximately $0.13 Z_{\odot}$.

We next examine whether the differences in metallicity could result from differences in star formation efficiency of CC and NCC groups, by determining the ratio of the group *B*-band luminosity to total group mass. For self-similar systems, total mass M scales as $T^{3/2}$, so we use the latter as a proxy for mass. We find $L_{B,group}/T^{3/2} = (1.57 \pm 0.18) \times 10^{11} L_{\odot,B} \text{ keV}^{-3/2}$ for the CC groups and $L_{B,group}/T^{3/2} = (2.02 \pm 0.45) \times 10^{11} L_{\odot,B} \text{ keV}^{-3/2}$ for the NCC groups. These values agree within their quoted standard errors, suggesting that CC and NCC systems are similarly efficient at forming stars. We can therefore exclude the possibility that NCC groups produce significantly fewer metals per unit total mass.

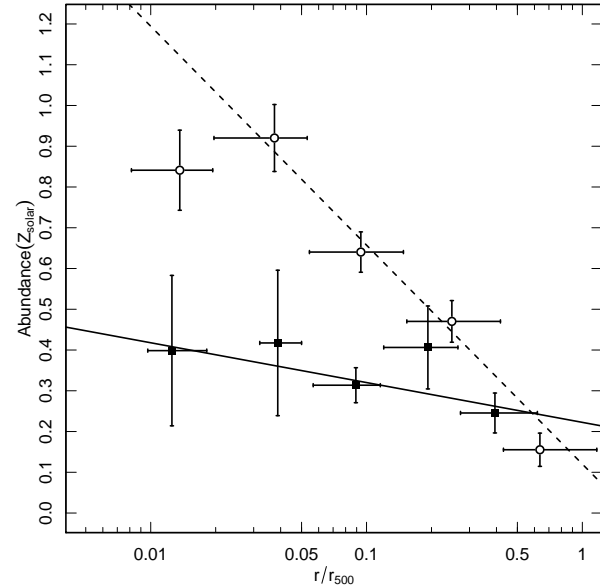


Figure 12. The stacked abundance profiles of the CC (open circles) and NCC sub-samples (filled squares) chosen to have the same mean temperatures. The vertical error bars show the standard error on the mean, and the horizontal error bars show the radial width of each bin. The dashed and solid lines are the linear fits to the whole data set of abundances shown in Figure 5.

Examining the gas mass weighted metal fraction in CC and NCC systems showed that if the central peak in NCC groups has been mixed out, we would expect an increase in metallicity at large radius in NCCs compared to CCs. There is no evidence for this given the limits of our data, implying that if the central peak has been mixed out, the metals have been pushed out past $0.5 r_{500}$. To fully resolve this issue would require detailed metallicity measurements at radii beyond $0.5 r_{500}$.

Taking an Occam’s Razor approach, we seek to identify a single cause for both the lack of cool cores and the flatter abundance profiles in NCC groups. Three possible mechanisms might account for the lack of cool cores in some groups – pre-heating, AGN mixing and merger disruption. We will now explore these three in detail, to see how they compare with observations. Feedback from supernova driven winds provides a fourth possible mechanism for suppressing cooling in the centres of groups. However, a higher level of such feedback would lead to an increased metal mass fraction, which is not observed, pointing instead to AGN feedback as the dominant feedback mechanism (Johnson et al. 2009). This conclusion was also reached by Diehl & Statler (2008), who found that although supernovae feedback can play a part in balancing radiative cooling in X-ray faint early-type galaxies, it is not the dominant mechanism in X-ray bright systems.

5.1 Pre-heating

One mechanism capable of preventing the formation of a cool core is strong initial pre-heating, which raises the entropy of the system to a level that prevents its cooling by the present day. This was proposed as a framework for understanding CC and NCC behaviour by McCarthy et al. (2008). However, if NCC groups were formed via pre-heating the system prior to group collapse as en-

visaged by the McCarthy et al. (2008) model, there is no reason why abundance gradients could not have built up since, as the estimated typical enrichment time required to build the central iron peak is ~ 5 Gyr (Rasmussen & Ponman 2009). This method is also inconsistent with the short central cooling times in NCC groups (O’Sullivan et al, in prep). It seems that we can therefore rule out pre-heating as a means capable, on its own, of preventing the formation of a CC, whilst accounting for the flat abundance gradients in NCC groups.

5.2 AGN mixing

AGN activity can re-distribute the metals in the ICM; for example, the entrainment of enriched gas has been observed in the Perseus (Sanders, Fabian & Dunn 2005) and Hydra A clusters (Kirkpatrick et al. 2009). In our sample, we see central flattening (or dips) in the abundance profiles of many CC groups, and there is some evidence that this flat region may extend further (to $\sim 0.1 r_{500}$) in the CC groups with a ‘radio-loud’ ($L_{1.4\text{GHz}} > 21.96 \text{ W Hz}^{-1}$) BGG, compared to an extent of $\sim 0.05 r_{500}$ around radio quiet BGGs. The abundance declines beyond these radii, suggesting that the effect of significant ongoing AGN activity in CC systems is to mix the ICM within the central ~ 50 kpc. These observations fit well with the AGN-driven circulation flow model of Mathews et al. (2004), which produces a central positive temperature gradient and a flat core in the iron abundance within ~ 50 kpc.

One potential difficulty with mixing gas out to $0.1 r_{500}$ in radio-loud CC groups is the required timescale. If the advection of enriched gas is restricted to velocities below the sound speed ($\sim 500 \text{ km s}^{-1}$ for a $T = 1 \text{ keV}$ system) then such mixing would take approximately 10^8 years. This is longer than most estimates of the duration of AGN outbursts. However, powerful FR II outbursts expand at supersonic velocities, generating lobes with typical size scales of 100 kpc (e.g. Shabala et al. 2008). With the current data we cannot probe the relationship between the current radio activity of the central BGG in NCC systems and their abundance profiles. However, the results of Diehl & Statler (2008), who found a lack of cool cores in elliptical galaxies with low radio luminosity, show that this is an important area for future study.

5.3 Mergers

Sanderson et al. (2006) find the NCC clusters in their sample to show evidence of recent disruption, favouring a merger hypothesis for their formation. Furthermore, Sanderson et al. (2009) have shown that weaker central cooling correlates with increased dynamical disturbance in clusters. Merging occurring on the group scale could therefore disrupt a cool core, and could potentially mix the metal distribution. We do find evidence for a significantly larger degree of substructure in the ICM of NCC groups, which could result from the impact of recent merger activity on the ICM. However, given the typically lower temperatures of NCC systems, the observation of greater entropy and pressure dispersion could alternatively be a reflection of the response of the ICM to the presence of individual galaxies. On the other hand, enhanced substructure could be an indicator of mixing processes, which need not necessarily be caused by mergers. With the current data there is no *unambiguous* sign of enhanced merger activity in NCC groups, but this is a promising area for further study.

On the basis of numerical simulations, Burns et al. (2008) propose that the early merger history of NCC clusters establishes their

gas properties, as major mergers destroy cool cores, leading to hot cores with long cooling times. However, this model fails in much the same way as the pre-heating models, as the observed short central cooling times in NCC groups and clusters (e.g. Sanderson et al. 2009, O’Sullivan et al, in prep.) and the lack of abundance gradients in NCC groups cannot be explained.

Simulations of merging galaxy clusters that initially host metallicity gradients by Poole et al. (2008) failed to mix the ICM sufficiently to wipe out the metallicity gradient. However, the presence of a high abundance region in HCG 62, approximately 34 kpc from the peak of the group X-ray emission provides observational evidence to support merger-induced metal mixing (Gu et al. 2007). It is true that Gu et al. (2007) cannot rule out AGN-induced mixing, and given the strong cool core in this system (Johnson et al. 2009), the merging activity appears not to have disrupted the cool core, or it occurred sufficiently long ago to allow the subsequent formation of a CC. It is possible that pre-heating could work in conjunction with mergers in NCCs to both prevent cooling and to mix the distribution of metals (I. G. McCarthy, private communication).

An alternative to *destruction* of a central abundance peak might be models in which the peak has not been established in the first place. Since much of the central peak is believed to originate from the BGG, this can be achieved if the BGG has not long been located at the centre of the group. This could be the case if NCC groups are dynamically young, and have only recently collapsed. This could also account for the presence of substructure in these systems. Even in older groups, it is worth noting that one consequence of a recent merger would be to displace the BGG from the group centre. Until the post-merger system settles down into a new virialised state, any new enriched gas from the galaxy will be distributed over a larger region than would be the case in an undisturbed group. The larger velocity offset of the BGG relative to the rest of the group seen in NCC groups compared to CC groups is consistent with this idea.

6 CONCLUSIONS

Using an *XMM-Newton* sample of 28 galaxy groups presented by Johnson et al. (2009), we have determined the mean abundance profiles of cool core (CC) and non cool core (NCC) systems. This is the first time that the abundance profiles of NCC groups have been examined in detail. Fitting a linear model in log–linear space to abundance profiles derived from two–temperature spectral fits, we find CC groups to exhibit steep abundance gradients with a slope of -0.54 ± 0.07 . We find generally good agreement between the abundance profiles of the CC groups and the abundance profiles of the *Chandra* group sample of Rasmussen & Ponman (2007), which was dominated by CC systems. However, fitting a linear model to the profiles of NCC groups yields a result consistent with a flat profile.

Examining the gas mass weighted mean metal fraction, the consequence of mixing out a central peak in the abundance profile of a NCC group would be a significant increase in metallicity compared to CC systems at large radii. However, there is no evidence for such an enhanced metallicity out to $0.5 r_{500}$, the limit of our data. To ascertain whether a central peak is simply mixed out to large radius in NCC systems requires mapping the metallicity of NCC groups at radii greater than $0.5 r_{500}$.

We investigate current AGN activity through the 1.4 GHz radio power of the brightest group galaxies (BGGs) in the groups, and find a significant anticorrelation between the core abundance gra-

dient and the radio power of the BGG within CC systems. Dividing the CC groups into ‘radio loud’ ($\log L_{1.4\text{GHz}} > 21.96 \text{ W Hz}^{-1}$) and ‘radio quiet’ ($\log L_{1.4\text{GHz}} \leq 21.96 \text{ W Hz}^{-1}$) subsamples shows both to have broadly similar abundance profiles. Central flattening in the typical abundance profiles may extend to larger radius ($\sim 0.1 r_{500}$) in radio-loud systems compared to radio-quiet systems ($\sim 0.05 r_{500}$). We interpret this as tentative evidence for AGN mixing within the central regions. Given the limits of the data, it is not possible to probe the behaviour of NCC abundance profiles in terms of the current radio activity of their BGGs.

The lack of cool cores and evidence for enhanced substructure in NCC groups suggests a disruptive event, whilst the short central cooling times and timescales for building a central metal peak indicate that this disruption has occurred within the past few Gyr. We favour merging as a likely mechanism consistent with the observations, although we cannot rule out powerful AGN outbursts as the drivers for group-wide mixing in NCC groups. The viability of powerful AGN outbursts in accounting for the properties of NCC groups could be tested by large statistical studies. It is also possible that some NCC groups are young systems, which have recently collapsed for the first time. Given the diverse properties of NCC groups, it is quite possible that they do not form a homogeneous class, and that a number of different effects are at work.

Critical questions for further investigation of NCC groups are to establish to what extent the presence of a currently active AGN affects their metallicity profiles, and whether enriched gas has been boosted to high entropy, by either mergers or AGN activity, and hence relocated to large radii in these groups.

ACKNOWLEDGMENTS

We thank the referee for their helpful comments, which have improved the paper. We thank Ian McCarthy for interesting discussions in relation to this project. RJ acknowledges support from STFC/PPARC and the University of Birmingham. JR acknowledges support by the Carlsberg Foundation. AF acknowledges support from BMBF/DLR under grants 50OR0207 and 50OR0204 to MPE. This research has made use of the NASA/IPAC Extragalactic Database (NED) which is operated by the Jet Propulsion Laboratory, California Institute of Technology, under contract with the National Aeronautics and Space Administration.

REFERENCES

- Allen S. W., Fabian A. C., Johnstone R. M., Arnaud K. A., Nulsen P. E. J., 2001, *MNRAS*, 322, 589
 Anders E., Grevesse N., 1989, *Geochim. Cosmochim. Acta*, 53, 197
 Arnaud M., Rothenflug R., Boulade O., Vigroux L., Vangioni-Flam E., 1992, *A&A*, 254, 49
 Baldi A., Ettori S., Mazzotta P., Tozzi P., Borgani S., 2007, *ApJ*, 666, 835
 Bird C. M., 1994, *AJ*, 107, 1637
 Buote D. A., 2000, *ApJ*, 539, 172
 Buote D. A., 1998, *MNRAS*, 296, 977
 Buote D. A., Lewis A. D., Brighenti F., Mathews W. G., 2003, *ApJ*, 595, 151
 Burns J. O., Hallman E. J., Gantner B., Motl P. M., Norman M. L., 2008, *ApJ*, 675, 1125
 Cleveland W. S., 1979, *JASA*, 74, 829
 Cleveland W. S., Grosse E., Shyu W., 1992, in Chambers J. M., Hastie T. J., eds, *Statistical Models in S*, Wadsworth & Brooks/Cole Advanced Books and Software, Chapt. 8
 Condon J. J., Cotton W. D., Broderick J. J., 2002, *AJ*, 124, 675
 Condon J. J., Cotton W. D., Greisen E. W., Yin Q. F., Perley R. A., Taylor G. B., Broderick J. J., 1998, *AJ*, 115, 1693
 Coziol R., Andernach H., Caretta C. A., Alamo-Martínez K. A., Tago E., 2009, *AJ*, 137, 4795
 Croston J. H., Hardcastle M. J., Birkinshaw M., 2005, *MNRAS*, 357, 279
 David L. P., Nulsen P. E. J., 2008, *ApJ*, 689, 837
 Diehl S., Statler T. S., 2008, *ApJ*, 687, 986
 De Grandi S., Molendi S., 2001, *ApJ*, 551, 153
 De Grandi S., Ettori S., Longhetti M., Molendi S., 2004, *A&A*, 419, 7
 Finoguenov A., Ponman T. J., 1999, *MNRAS*, 305, 325
 Finoguenov A., Davis D. S., Zimer M., Mulchaey J. S., 2006, *ApJ*, 646, 143
 Finoguenov A., Ponman T. J., Osmond J. P. F., Zimer M., 2007, *MNRAS*, 374, 737
 Giodini S., et al., 2009, *ApJ*, 703, 982
 Gonzalez A. H., Zaritsky D., Zabludoff A. I., 2007, *ApJ*, 666, 147
 Grevesse N., Sauval A. J., 1998, *SSRv*, 85, 161
 Gu J., Xu H., Gu L., An T., Wang Y., Zhang Z., Wu X.-P., 2007, *ApJ*, 659, 275
 Gunn J. E., Gott J. R., III, 1972, *ApJ*, 176, 1
 Jetha N. N., Ponman T. J., Hardcastle M. J., Croston J. H., 2007, *MNRAS*, 376, 193
 Johnson R., Ponman T. J., Finoguenov A., 2009, *MNRAS*, 395, 1287
 Kirkpatrick C. C., Gitti M., Cavagnolo K. W., McNamara B. R., David L. P., Nulsen P. E. J., Wise M. W., 2009, *ApJ*, 707, L69
 Kochanek C. S., et al., 2001, *ApJ*, 560, 566
 Komiyama M., Sato K., Nagino R., Ohashi T., Matsushita K., 2009, *PASJ*, 61, 337
 Lin Y.-T., Mohr J. J., 2004, *ApJ*, 617, 879
 McCarthy I. G., Babul A., Bower R. G., Balogh M. L., 2008, *MNRAS*, 386, 1309
 Mahdavi A., Finoguenov A., Böhringer H., Geller M. J., Henry J. P., 2005, *ApJ*, 622, 187
 McNamara B. R., Nulsen P. E. J., 2007, *ARA&A*, 45, 117
 Mathews W. G., Brighenti F., Buote D. A., 2004, *ApJ*, 615, 662
 Moll R., et al., 2007, *A&A*, 463, 513
 Morita U., Ishisaki Y., Yamasaki N. Y., Ota N., Kawano N., Fukazawa Y., Ohashi T., 2006, *PASJ*, 58, 719
 Peres C. B., Fabian A. C., Edge A. C., Allen S. W., Johnstone R. M., White D. A., 1998, *MNRAS*, 298, 416
 Poole G. B., Babul A., McCarthy I. G., Sanderson A. J. R., Fardal M. A., 2008, *MNRAS*, 391, 1163
 R Development Core Team 2008, *R: A Language and Environment for Statistical Computing*, R Foundation for Statistical Computing, Vienna, Austria
 Rasera Y., Lynch B., Srivastava K., Chandran B., 2008, *ApJ*, 689, 825
 Rasmussen J., Ponman T. J., 2007, *MNRAS*, 380, 1554 (RP07)
 Rasmussen J., Ponman T. J., 2009, *MNRAS*, 399, 239
 Rebusco P., Churazov E., Böhringer H., Forman W., 2006, *MNRAS*, 372, 1840
 Sanders J. S., Fabian A. C., Dunn R. J. H., 2005, *MNRAS*, 360, 133
 Sanderson A. J. R., Ponman T. J., O’Sullivan E., 2006, *MNRAS*, 372, 1496

- Sanderson A. J. R., O'Sullivan E., Ponman T. J., 2009, MNRAS, 395, 764
- Sanderson A. J. R., Edge A. C., Smith G. P., 2009, MNRAS, 398, 1698
- Sato K., Matsushita K., Ishisaki Y., Yamasaki N. Y., Ishida M., Ohashi T., 2009, PASJ, 61, 353
- Schindler S., Diaferio A., 2008, SSRv, 134, 363
- Shabala S. S., Ash S., Alexander P., Riley J. M., 2008, MNRAS, 388, 625
- Sivanandam S., Zabludoff A. I., Zaritsky D., Gonzalez A. H., Kelson D. D., 2009, ApJ, 691, 1787
- Skrutskie M. F., et al., 2006, AJ, 131, 1163
- Sun M., Voit G. M., Donahue M., Jones C., Forman W., Vikhlinin A., 2009, ApJ, 693, 1142
- Tokoi K., et al., 2008, PASJ, 60, 317
- Voigt L. M., Fabian A. C., 2004, MNRAS, 347, 1130